Journal of Materials Chemistry A

PAPER

View Article Online
View Journal | View Issue



Cite this: J. Mater. Chem. A, 2016, 4, 15081

# Two heterovalent copper–organic frameworks with multiple secondary building units: high performance for gas adsorption and separation and $I_2$ sorption and release†

Shuo Yao,[a] Xiaodong Sun,[a] Bing Liu,[a] Rajamani Krishna,[b] Guanghua Li,[a] Qisheng Huo[a] and Yunling Liu*[a]

Received 20th June 2016
Accepted 4th September 2016

DOI: 10.1039/c6ta05142a

www.rsc.org/MaterialsA

With the help of the multiple secondary building unit (SBU) strategy, two novel heterovalent Cu–MOFs, $[(Cu_4I_4)Cu_4L_4(DABCO)_2]\cdot16DMF$ (JLU-Liu31) and $[(Cu_4I_4)Cu_3L_3(DABCO)(DMF)_2]\cdot18DMF$ (JLU-Liu32) [$H_2L$ = pyridine-3,5-bis(phenyl-4-carboxylic acid), DABCO = 1,4-diazabicyclo[2.2.2]-octane], have been successfully solvothermally synthesized and structurally characterized. Both of the two compounds feature multiple SBUs and exhibit novel topologies. JLU-Liu31 possesses the largest sustainable pore volume among the MOFs based on $Cu_4I_4$ clusters. Moreover, the adsorption behaviours of the desolvated JLU-Liu31 material for some small gases ($H_2$, $O_2$, $CO_2$, $CH_4$, $C_2H_6$ and $C_3H_8$) have been analysed in low pressure regions; meanwhile, it exhibits commendable selectivity for $O_2$ over $N_2$, and $C_3H_8$ over $CH_4$. The remarkable results illustrate that JLU-Liu31 is a good candidate for application in the separation of light hydrocarbons. Additionally, JLU-Liu32 exhibits impressive performance for $I_2$ sorption and release in solvents.

## Introduction

Light hydrocarbons are widely utilized as important raw materials and energy sources for industrial products and fine chemicals. Methane as the basis of natural gas is considered to be a preferable candidate for a more clean energy source for generating the smallest amount of $CO_2$ for each unit of heat.[1] Although ethane and propane significantly enhance the value as petrochemical feedstock, they are impurities of natural gas and reduce the conversion rate.[2] Furthermore, the addition of oxygen to fuel streams can improve the combustion efficiency at the same time. Feedstock oxygen is currently produced by cryogenic air separation of $O_2$ over competing air component $N_2$, which is expensive and energy consuming.[3] Therefore, it is important to develop materials with efficient selectivity to purify natural gases and separate oxygen from nitrogen in the air.

Metal–organic frameworks as a type of burgeoning materials, which possess fascinating diversity of architectures and great prospects to approach the challenges in the applications of gas adsorption and separation, luminescence sensing, and catalysis, provide us the impetus to actively pursue them over the past two decades.[4] A variety of synthesis strategies are put forward to design and synthesize MOFs with good performance for gas adsorption and separation, such as secondary building units (SBUs),[5] open metal sites (OMSs),[6] Lewis basic sites (LBSs),[7] ionic skeletons[8] and so forth. Of these strategies, the SBU strategy is a powerful way to fabricate MOFs. The clusters of Cu-paddlewheels and $Cu_4I_4$ are the classical SBUs in the MOF family. We are looking forward to acquiring frameworks with the two kinds of SBUs simultaneously. It is widely known that a Cu-paddlewheel is coordinated to four carboxylate groups and the terminal coordinated groups can be solvent molecules or N-containing ligands. In addition, $Cu_4I_4$ clusters prefer to coordinate to four N atoms.[9] Based on the above considerations, we choose heterofunctional pyridine-3,5-bis(phenyl-4-carboxylic acid) ($H_2L$) as an organic ligand which contains both carboxylate and pyridyl groups. Since the Cu ions in the two kinds of SBUs have different valence states, we use CuI as the metal source which possesses monovalent copper and is easily oxidized to bivalent. It is worth noting that MOFs with a novel topology and huge porosity can be achieved by employing mixed ligands.[10] Accordingly, 1,4-diazabicyclo[2.2.2]-octane (DABCO) as a second ligand is introduced into the above system to construct the

[a]State Key Laboratory of Inorganic Synthesis and Preparative Chemistry, College of Chemistry, Jilin University, Changchun 130012, P. R. China. E-mail: yunling@jlu.edu.cn; Fax: +86-431-85168624; Tel: +86-431-85168614

[b]Van 't Hoff Institute for Molecular Sciences, University of Amsterdam, Science Park 904, 1098 XH Amsterdam, The Netherlands. E-mail: r.krishna@contact.uva.nl

† Electronic supplementary information (ESI) available: Materials and methods, crystal data and structure refinement, structure information, XRD, TGA, gas adsorption and adsorption selectivity. CCDC 1480153 and 1480154. For ESI and crystallographic data in CIF or other electronic format see DOI: 10.1039/c6ta05142a

framework. Fortunately, we successfully prepare two intriguing heterovalent copper–organic frameworks $[(Cu_4I_4)Cu_4L_4(DABCO)_2]\cdot 16DMF$ (JLU-Liu31) and $[(Cu_4I_4)Cu_3L_3(DABCO)(DMF)_2]\cdot 18DMF$ (JLU-Liu32), which are made up of multiple SBUs. Additionally, both of them exhibit novel topologies that have been accessed for the first time. JLU-Liu31 can provide the largest sustainable pore volume among the MOFs based on $Cu_4I_4$ clusters. Moreover, the adsorption behaviour of the desolvated JLU-Liu31 material for some other small gases ($H_2$, $O_2$, $CO_2$, $CH_4$, $C_2H_6$, $C_3H_8$) has been analysed. Ideal adsorbed solution theory (IAST) calculations and breakthrough simulations have also been performed to investigate the gas selectivity in low pressure regions. The commendable results illustrate that JLU-Liu31 is a good candidate for application in light hydrocarbon purification. Because JLU-Liu32 is not stable after removing the guest molecules, it only exhibits impressive $I_2$ sorption and release performance in solvent.

# Experimental

### Materials and methods

All chemicals were obtained from commercial sources and used without further purification. Powder X-ray diffraction (PXRD) data were collected on a Rigaku D/max-2550 diffractometer with Cu $K_\alpha$ radiation ($\lambda = 1.5418$ Å). Elemental analyses (C, H, and N) were performed by using a vario MICRO (Elementar, Germany). Thermal gravimetric analyses (TGA) were performed on a TGA Q500 thermogravimetric analyzer used in air with a heating rate of 10 °C $min^{-1}$. The liquid state UV-vis spectra were recorded on a SHIMADZU UV-2450 UV-visible spectrophotometer within 200–700 nm by using the same solvent as the blank.

### Synthesis of JLU-Liu31

CuI (12 mg 0.06 mmol) and $H_2L$ (4 mg, 0.01 mmol) were added to *N*,*N*-dimethylformamide (DMF) (2 mL)/DABCO (0.1 mL) with $HNO_3$ (0.2 mL) (2.2 mL $HNO_3$ in 10 mL DMF). The mixture was kept at room temperature for 6 hours until the colour became dark brown. Single crystals of JLU-Liu31 were obtained when the mixture was heated at 85 °C for 24 hours. Green stick crystals were obtained and air-dried (yield 50%, based on $H_2L$). Elemental analysis (%) Calcd for JLU-Liu31 $[(Cu_4I_4)Cu_4L_4(DABCO)_2]\cdot 16DMF$: C, 44.40; H, 4.93; N, 9.14; found: C, 43.82; H, 4.79; N, 8.81. The experimental PXRD pattern is in good agreement with the simulated one based on the single-crystal X-ray data, indicating the purity of the as-synthesized product (Fig. S1†).

### Synthesis of JLU-Liu32

A mixture of CuI (18 mg 0.095 mmol), $H_2L$ (5 mg, 0.015 mmol), DMF (1 mL), DABCO (0.2 mL) and $HNO_3$ (0.3 mL) (2.2 mL $HNO_3$ in 10 mL DMF) was sealed into a 20 mL capped vial and kept for 6 hours at room temperature until it became dark brown. The mixture was heated at 85 °C for 24 hours and blue block crystals of JLU-Liu32 were obtained. The crystals were collected and washed with DMF (yield 55%, based on $H_2L$). Elemental analysis calcd (%) for JLU-Liu32, $[(Cu_4I_4)Cu_3L_3(DABCO)(DMF)_2]\cdot 18DMF$: C, 42.13; H, 5.32; N, 10.79; found: C, 41.24; H, 5.20; N, 10.98. The experimental PXRD pattern agrees well with the simulated one based on the single-crystal X-ray data, indicating the purity of the as-synthesized product (Fig. S2†).

### X-ray crystallography

Crystallographic data for two compounds were collected on a Bruker Apex II CCD diffractometer using graphite-monochromated Mo-K$\alpha$ ($\lambda = 0.71073$ Å) radiation at room temperature. The structures were solved by direct methods and refined by full-matrix least-squares on $F^2$ using version 5.1.[11] All the metal atoms were located first, and then the oxygen and carbon atoms of the compound were subsequently found in difference Fourier maps. The hydrogen atoms of the ligand were placed geometrically. All non-hydrogen atoms were refined anisotropically. The final formula was derived from crystallographic data combined with elemental and thermogravimetric analysis data. The detailed crystallographic data are listed in Table S1.† Crystallographic data for JLU-Liu31 (1480153) and JLU-Liu32 (1480154) have been deposited with Cambridge Crystallographic Data Centre. Topology information for the two compounds was calculated by using TOPOS 4.0.[12]

### Gas adsorption measurements

$N_2$, $H_2$, $O_2$, $CO_2$, $CH_4$, $C_2H_6$ and $C_3H_8$ gas adsorption measurements were performed on Micromeritics ASAP 2420, Micromeritics ASAP 2020 and Micromeritics 3-Flex instruments. Before gas adsorption measurements, JLU-Liu31 was exchanged with fresh acetone 10 times for 2 days and JLU-Liu32 was exchanged with fresh ethanol to completely remove the non-volatile solvent molecules, which can be proved by TGA analysis (Fig. S3 and S4†). The samples were activated by drying under dynamic vacuum at room temperature for 1 hour. Before the measurement, the sample was dried again by using the 'outgas' function of the surface area analyzer for 10 h at 100 °C.

# Results and discussion

### Crystal structure descriptions

Single-crystal X-ray diffraction analysis shows that JLU-Liu31 crystallizes in the orthorhombic crystal system with the space group of *Cmcm*. As shown in Fig. 1a, JLU-Liu31 consists of ternary SBUs: an organic SBU formed by 3-connected ligands which contain carboxyl and pyridyl groups; an inorganic SBU composed of familiar paddlewheels which possess four carboxyl groups from four ligands and two terminal coordinated DABCO groups; an inorganic SBU constructed by the cluster of $Cu_4I_4$ which coordinates to four pyridyl groups from four ligands. Fig. 1b distinctly illustrates the formation of the 3D framework. The copper paddlewheels are weaved by ligands to configure 2D layers, and the 2D layers are further bridged by $Cu_4I_4$ clusters to fabricate the 3D framework. Meanwhile, the DABCO ligands join the adjacent paddlewheels to doubly support the framework and to a considerable extent increase the rigidity of the framework. Although the supporting DABCO reduces the window size of the framework, it still contains a relatively large one-dimensional channels with a diameter of 11.4 Å × 9.6 Å and a small one with 2.5 Å × 4.3 Å considering the van der

 

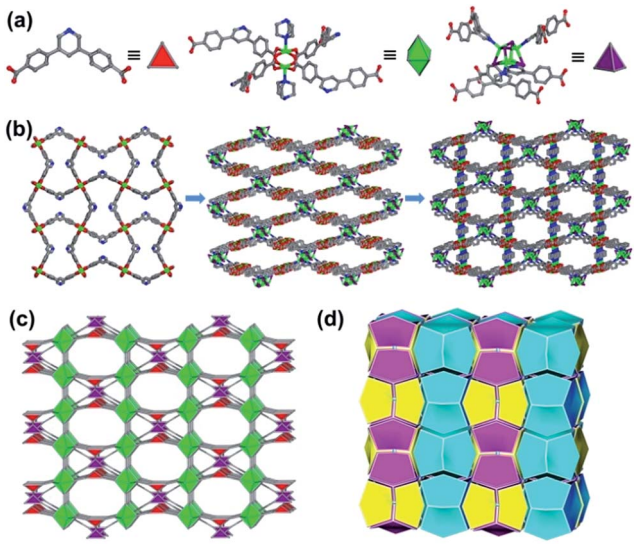


Fig. 1 Single-crystal structure of JLU-Liu31: (a) ternary SBUs consisting of ligand and metal cores. (b) The formation of a 3D framework from a 2D layer and the double reinforcement of the structure by DABCO. (c) Polyhedral view of the framework. (d) Topological features of the compound displayed by tiles.

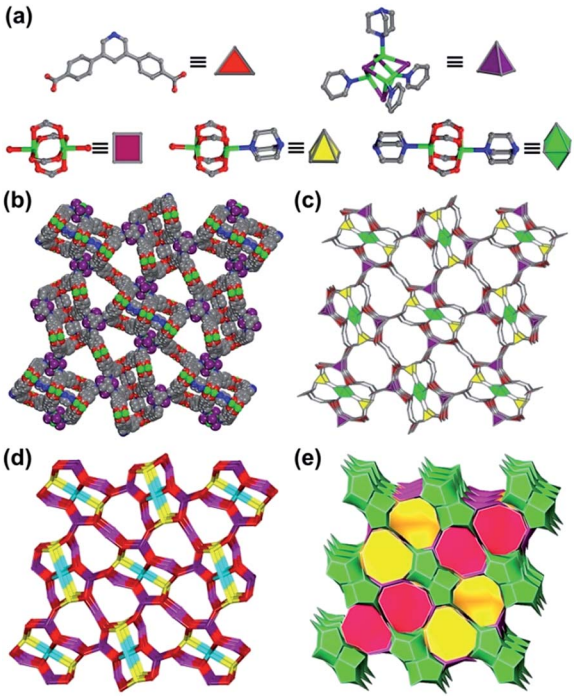


Fig. 2 Single-crystal structure of JLU-Liu32: (a) multiple SBUs consisting of ligand and metal cores. (b) The space-filling model of the channel along the [001] direction. (c) Polyhedral view of the framework. (d) The new type of topology. (e) Topological features of the compound displayed by tiles.

Waals radius. From a topological point of view, the ligand is regarded as a 3-connected node with a triangular geometry, the terminal coordinated paddlewheel can be seen as a 6-connected node with an octahedral geometry and the $Cu_4I_4$ cluster is considered as a 4-connected node with a tetrahedral geometry. Consequently, the structure of JLU-Liu31 can be described as a (3, 4, 6)-connected network with a Schläfli symbol of $(5^2\cdot6)_4(5^4\cdot6^2)(5^4\cdot6^8\cdot8\cdot9^2)_2$, which has been accessed for the first time (Fig. 1c and Table S2†). Furthermore, the topological features displayed by tiles are shown in Fig. 1d and S5.† The overall topology is made up of three types of tiles of $[5^2\cdot6^2]$, $[5^2\cdot6^2]$ and $[6^8]$. The PLATON calculation reveals a total solvent-accessible volume of 14 986.3 $Å^3$ per unit cell, which accounts for approximately 71.5% of the cell volume, exhibiting high porosity and offering possibilities for gas adsorption.

The X-ray crystallographic analysis revealed that JLU-Liu32 crystallizes in the orthorhombic crystal system with the space group of *Pnnm*. As can be seen in Fig. 2a, JLU-Liu32 possesses more pluralistic systems of quinary SBUs: the same organic SBU as JLU-Liu31 and four types of inorganic SBUs. The four types of inorganic SBUs are composed of a 4-connected classical paddlewheel, a 5-connected paddlewheel with one terminal coordinated DABCO group, a 6-connected paddlewheel with two terminal coordinated DABCO groups and a cluster of $Cu_4I_4$ which coordinates to three pyridyl groups from three ligands and one DABCO group. Fig. 2b shows the space-filling model of JLU-Liu32 which can illustrate the window size of the channel along the [001] direction distinctly. Five types of SBUs can be simplified as triangular, tetrahedral, square, pyramidal and octahedral geometries. Therefore, the overall structure of JLU-Liu32 possesses a new type of topology with a Schläfli symbol of $(5^2\cdot8^2\cdot11^2)(5^2\cdot8)_8(5^3\cdot8^3)_2(5^3)_4(5^4\cdot8^2)_4(5^5\cdot8^5)_2(5^8\cdot8^7)$ (Fig. 2c and d and Table S2†). As represented in Fig. 2e and S6,† there are four kinds of tiles of $[5^6\cdot8^2]$, $[5^2\cdot8^2]$, $[5^2\cdot8^2\cdot10^2]$ and $[5^4\cdot8^2\cdot10^2]$. The PLATON calculation reveals a total solvent-accessible volume of 31 719.7 $Å^3$ per unit cell, which accounts for approximately 78.2% of the cell volume.

## Thermal gravimetric analyses (TGA)

TGA was carried out to evaluate the thermal stability of the two compounds and the pore volume which was occupied by guest molecules under atmospheric environment. It turns out that the framework of JLU-Liu31 can be stable up to about 280 °C with approximately 45% weight loss before 200 °C owing to the removal of guest molecules (Fig. S3†). JLU-Liu32 is stable up to 300 °C with approximately 40% weight loss observed before 200 °C because of the removal of guest molecules (Fig. S4†). It is obvious that both of the two compounds exhibit more prominent pore volume and good thermal stability than InOF-8 (ref. 13) and COZ-1 (ref. 14) which both comprise $Cu_4I_4$ clusters.

## Gas adsorption and separation behaviours

It is generally known that the four coordination bonds which are formed by $Cu_4I_4$ cluster and nitrogen containing groups don't have enough strength to support the framework when the guest molecules are removed. Therefore, only few reported MOFs with $Cu_4I_4$ clusters possess good performance for gas adsorption.[13–15] Although the permanent porosity of COZ-1 can be confirmed by $N_2$ sorption measurements, the experimental pore volume is much lower than the theoretical one which can

be ascribed to the integrity loss of the framework. Benefiting from the $Cu_4I_4$ cluster and DABCO double supporting the framework simultaneously as a fence, JLU-Liu31 shows commendable gas adsorption behaviour. The permanent porosity and surface areas of activated JLU-Liu31 were investigated by reversible $N_2$ sorption experiments at 77 K. The $N_2$ adsorption of activated JLU-Liu31 reveals a reversible type-I isotherm characteristic which is the nature of microporous materials (Fig. 3). The BET surface area and Langmuir surface area of JLU-Liu31 were calculated to be 1700 $m^2\ g^{-1}$ and 2300 $m^2\ g^{-1}$, respectively. To the best of our knowledge, JLU-Liu31 shows the highest surface area among the MOFs or inorganic–organic materials based on $Cu_4I_4$ SBUs. The experimental micropore volume is 0.85 $cm^3\ g^{-1}$ which is close to the theoretical value of 0.95 $cm^3\ g^{-1}$. The close numerical values indicate that the pores in JLU-Liu31 are able to keep its integrity and ensure its good adsorption performance. Although JLU-Liu32 exhibits high performance in terms of pore volume and thermal stability from analysing the structure and TGA, there is almost no $N_2$ adsorption. This can be attributed to the fact that the whole 3D framework of JLU-Liu32 is only propped up by $Cu_4I_4$ clusters and it will collapse after the removal of guest molecules or upon activation under vacuum. On the basis of the above reasons, JLU-Liu32 is not an appropriate candidate material for gas adsorption.

In the light of the high stability and surface area of JLU-Liu31, we investigate its adsorption performance for some other small gases. In comparison with nitrogen, oxygen is also a kind of diatomic gas molecule with a similar dynamic radius ($N_2$: 3.64 Å, $O_2$: 3.46 Å). Consequently, it is not easy to achieve the separation of them and seldom reported MOF materials are related to the highly selective separation of $O_2$ over $N_2$.[16] We investigate the capacity of oxygen adsorption for JLU-Liu31. The results indicate that the maximum adsorption amount of $O_2$ is 700 $cm^3\ g^{-1}$ at 77 K (Fig. 3), which is significantly higher than that of other highly porous MOFs.[17] In comparing with $N_2$ gas sorption isotherms measured under the same conditions, $O_2$ is more favourably adsorbed over $N_2$ with an $O_2/N_2$ selectivity of 1.34 at $0.2P/P_0$. The $O_2/N_2$ selectivity of JLU-Liu31 is higher than those of Fe/Cu-BTC and Co/Cu-BTC with open metal sites (OMSs)[18] and JLU-Liu18 without OMSs.[19] Most reported MOFs with high $O_2/N_2$ selectivity can be ascribed to the following: (i) $O_2$ can side-on or end-on coordinate to the OMSs, and (ii) the pore size ranges between the kinetic diameter of $O_2$ and $N_2$. For JLU-Liu31, the unique pore size and shape induce the high selectivity collaboratively. Low-pressure uptake of $H_2$ is also detected and the adsorption amount is 1.17 wt% (131 $cm^3\ g^{-1}$) and 0.54 wt% (61 $cm^3\ g^{-1}$) at 77 and 87 K under 1 bar, respectively (Fig. S8†), which are comparable with those of reported MOFs.[20] At low coverage, the isosteric heat ($Q_{st}$) of JLU-Liu31 for $H_2$ is 8 kJ $mol^{-1}$.

The $CO_2$ adsorption performance was explored and the adsorption isotherms are shown in Fig. 4. The amount of $CO_2$ uptake for JLU-Liu31 is 35 and 17 $cm^3\ g^{-1}$ at 273 and 298 K under 1 bar, respectively. To make a thorough inquiry for the interaction between $CO_2$ and the framework, the behaviour of the isosteric heat was analysed. At zero loading, the adsorption enthalpy of JLU-Liu31 is 32.6 kJ $mol^{-1}$ (Fig. S9†). Albeit the amount of $CO_2$ adsorption is normal, its $Q_{st}$ is relatively higher than that of dia-7i-1-Co[21] and slightly lower than that of HKUST-1.[22] The potential storage and selective separation applications for some light hydrocarbons of $CH_4$, $C_2H_6$ and $C_3H_8$, which are the primary compositions of flue gas, natural gas and biogas, are also evaluated at 273 and 298 K under 1 bar, respectively. The maximum adsorption of $CH_4$ is 14 and 8 $cm^3\ g^{-1}$, $C_2H_6$ is 142 and 68 $cm^3\ g^{-1}$ and $C_3H_8$ is 191 and 169 $cm^3\ g^{-1}$, respectively (Fig. 4). Furthermore, the $Q_{st}$ of $CH_4$, $C_2H_6$ and $C_3H_8$ is 13, 25 and 20 kJ $mol^{-1}$, respectively, as estimated from the sorption isotherms at 273 and 298 K (Fig. S10–S12†).

In the interest of assessing the practical separation ability of JLU-Liu31 for $CO_2$, the theoretical separation of $CO_2/CH_4$ (5% and 95%, 50% and 50%) is analysed by using the IAST model which is a common method to predict binary mixture gas adsorption from experimental single-component isotherms. Adopting the dual-site Langmuir–Freundlich equation, we successfully fit the data and the model fits the isotherms at 298 K very well ($R^2$ > 0.9999) (Fig. 5a).[23] Afterward, the fitting

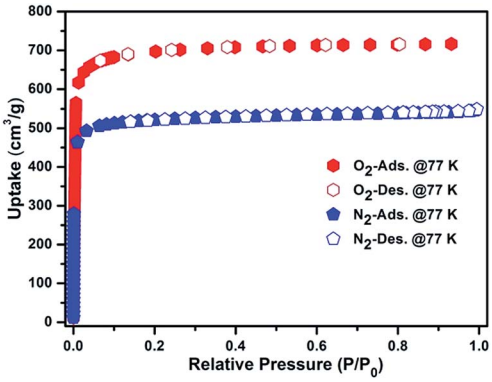


Fig. 3 Oxygen (red) and nitrogen (blue) sorption isotherms of JLU-Liu31 at 77 K.

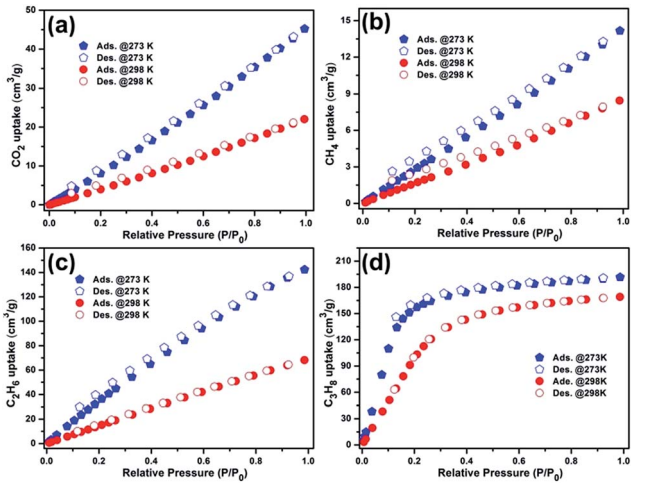


Fig. 4 (a) $CO_2$; (b) $CH_4$; (c) $C_2H_6$; (d) $C_3H_8$ gas sorption isotherms of JLU-Liu31 at 273 and 298 K under 1 bar.

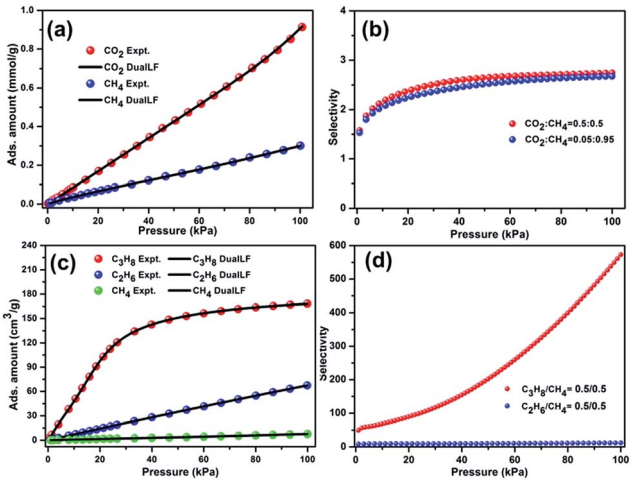


Fig. 5 $CO_2$, $CH_4$, $C_2H_6$ and $C_3H_8$ adsorption isotherms at 298 K along with the dual-site Langmuir Freundlich (DSLF) fits (a, c); gas mixture adsorption selectivity is predicted by IAST at 298 K and 100 kPa for JLU-Liu31 (b, d).

parameters are used to predict multi-component adsorption by IAST (Table S5†). At 298 K and 1 bar, the selectivity of JLU-Liu31 for $CO_2$ over $CH_4$ is 2.7 and 2.6 (Fig. 5b), which are comparable to the values of ZIF-8 and some carbon materials under the same measurement conditions.[24] The potential application for the separation of industrial light hydrocarbons is also investigated for JLU-Liu31 by IAST. The same fitting method is employed to achieve the fitting parameters (Fig. 5c and Table S5†). As shown in Fig. 5d, the selectivity for $C_2H_6$ over $CH_4$ and $C_3H_8$ over $CH_4$ for equimolar is 12 and 573 at 298 K and 1 bar, respectively. It is worth mentioning that the selectivity for $C_3H_8$ over $CH_4$ is much higher than the very high value of UTSA-35a[25] and FJI-C1.[26]

The performance of industrial fixed bed adsorbers is dictated by a combination of adsorption selectivity and uptake capacity. To further demonstrate the separation potential of JLU-Liu31, we performed transient breakthrough simulations using the simulation methodology described in the literature.[27] For the breakthrough simulations, the following parameter values were used: length of the packed bed, $L = 0.3$ m; voidage of the packed bed, $\varepsilon = 0.4$; superficial gas velocity at the inlet, $u = 0.04$ m s$^{-1}$. We investigated the simulation results for the transient breakthrough of an equimolar 4-component $CH_4/CO_2/C_2H_6/C_3H_8$ mixture and 3-component $CH_4/C_2H_6/C_3H_8$ mixture in a fixed bed packed with JLU-Liu31 operating at a total pressure of 100 kPa and 298 K (Fig. 6). The transient breakthrough simulation results are presented in terms of dimensionless time, $\tau$, defined by dividing the actual time, $t$, by the characteristic time, $L\varepsilon/u$. The $y$-axis represents the dimensionless concentration of the components at the exit of the fixed bed adsorber. The results indicate that JLU-Liu31 is suitable for selective adsorption of propane from the four component gas mixture and fractionating a mixture of C1/C2/C3 hydrocarbons into three fractions.

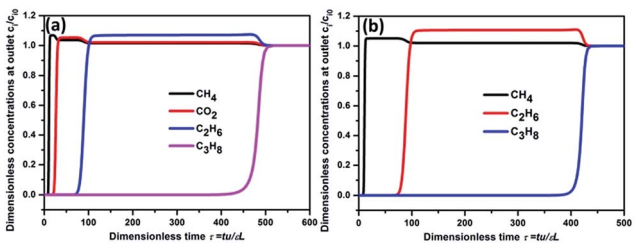


Fig. 6 Simulations of transient breakthrough characteristics for an equimolar 4-component $CH_4/CO_2/C_2H_6/C_3H_8$ mixture (a) and equimolar 3-component $CH_4/C_2H_6/C_3H_8$ mixture (b) in JLU-Liu31 at 100 kPa and 298 K.

## Iodine adsorption and desorption experiments

Both of the two compounds are evaluated with respect to their abilities of sorption and release of iodine in solvents. Before the measurement, JLU-Liu31 is solvent exchanged with acetone for 2 days, while the exchanging solvent for JLU-Liu32 is ethanol. Then, 100 mg of the activated samples are soaked in 3 mL cyclohexane solution of $I_2$ (0.01 M) in a sealed vial and kept at room temperature. As illustrated in Fig. 7a and S13a,† the $I_2$ adsorption process can be observed with the colour fading from claret red to light pink after 24 h in a cyclohexane solution of $I_2$. Additionally, Fig. 7b and S13b† present the $I_2$ release processes with a colour change to dark brown after 12 h of immersion of 20 mg $I_2$-adsorbed samples in ethanol. The total adsorption value of $I_2$ in molecules per formula unit is 3.65 and 4 for JLU-Liu31 and JLU-Liu32. It is noteworthy that the uptakes of $I_2$ being adsorbed per formula unit are lower than those of ZIF-8 (ref. 28) while higher than those of $\{(Cu_2I_2)$(tetra-4-(4-pyridyl) phenylmethane)$]\cdot$solvent$\}_n$[29] and $\{[Zn_3$(D-Llac)$_2$(pybz)$_2]\cdot 3I_2\}_n$.[30]

The release dynamic process can also be detected by using the UV-vis spectra. As represented in Fig. 8, the evolution of UV-vis spectra showed $\lambda_{max}$ at 204, 231, and 360 nm which should be ascribed to the concentration of $I_2$ and polyiodide $I_3^-$. The inserts in Fig. 8 show the $I_2$ release rate of the compounds in ethanol, which are plotted as the absorption intensity at 231 nm versus time. For the two compounds, the release of $I_2$

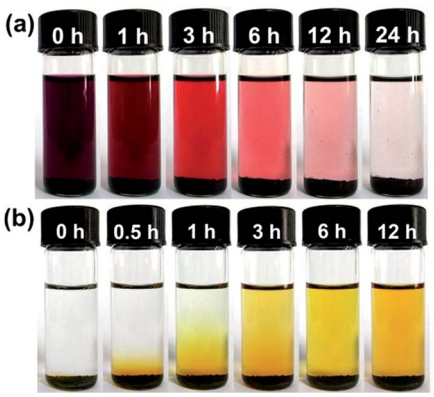


Fig. 7 (a) Photographs of the time-dependent $I_2$ adsorption process of 100 mg JLU-Liu32 in 3 mL cyclohexane. (b) Photographs of the time-dependent $I_2$ release process of 20 mg JLU-Liu32 in 3 mL ethanol.

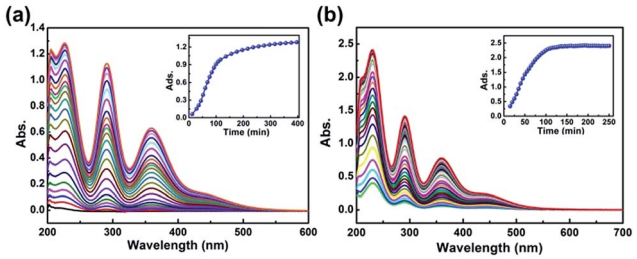


Fig. 8 UV-vis spectra of $I_2$ release in ethanol for JLU-Liu31 (a) and JLU-Liu32 (b). The insets are dynamic intensity (monitored at 231 nm) *vs.* time plots.

increases sharply and then gently. However, JLU-Liu32 ($2.3 \times 10^{-6}$ mol $L^{-1}$ $min^{-1}$) releases the iodine more quickly than JLU-Liu31 ($8.5 \times 10^{-7}$ mol $L^{-1}$ $min^{-1}$) according to the standard curve (Fig. S14 and S15†), which is faster than JLU-Liu15.[31] The notable performance of JLU-Liu32 for $I_2$ sorption and release is governed by its outstanding porosity which is more open than that of JLU-Liu31.

## Conclusions

In summary, by adopting the powerful synthesis strategy of multiple SBUs, we have successfully solvothermally synthesized and structurally characterized two novel heterovalent Cu–MOFs based on a tridentate heterofunctional ligand and a secondary DABCO ligand. Both of the two compounds feature multiple SBUs and novel topologies. JLU-Liu31 possesses the largest sustainable pore volume among the MOFs based on $Cu_4I_4$ clusters and exhibits notable adsorption for some small gases and light hydrocarbons. Meanwhile, it displays preferable selectivity for $O_2$ over $N_2$, and $C_3H_8$ over $CH_4$ as well. In addition, JLU-Liu32 exhibits impressive performance for $I_2$ sorption and release in solvents.

## Acknowledgements

This work was supported by the National Natural Science Foundation of China (No. 21373095 and 21371067).

## Notes and references

1 P. Nugent, Y. Belmabkhout, S. D. Burd, A. J. Cairns, R. Luebke, K. Forrest, T. Pham, S. Ma, B. Space, L. Wojtas, M. Eddaoudi and M. J. Zaworotko, *Nature*, 2013, **495**, 80–84; Y. He, W. Zhou, T. Yildirim and B. Chen, *Energy Environ. Sci.*, 2013, **6**, 2735–2744; Y. He, W. Zhou, G. Qian and B. Chen, *Chem. Soc. Rev.*, 2014, **43**, 5657–5678.

2 S. Chaemchuen, N. A. Kabir, K. Zhou and F. Verpoort, *Chem. Soc. Rev.*, 2013, **42**, 9304–9332; I. Spanopoulos, C. Tsangarakis, E. Klontzas, E. Tylianakis, G. Froudakis, K. Adil, Y. Belmabkhout, M. Eddaoudi and P. N. Trikalitis, *J. Am. Chem. Soc.*, 2016, **138**, 1568–1574; D. M. D'Alessandro, B. Smit and J. R. Long, *Angew. Chem., Int. Ed.*, 2010, **49**, 6058–6082; H. Wu, Q. Gong, D. H. Olson and J. Li, *Chem. Rev.*, 2012, **112**, 836–868.

3 N. A. Khan, S. Shaikhutdinov and H.-J. Freund, *Catal. Lett.*, 2006, 108; A. R. Smith and J. Klosek, *Fuel Process. Technol.*, 2001, **70**, 115.

4 Y. Cui, B. Li, H. He, W. Zhou, B. Chen and G. Qian, *Acc. Chem. Res.*, 2016, **49**, 483–493; H. Li, M. Eddaoudi, M. O'Keeffe and O. M. Yaghi, *Nature*, 1999, **402**, 276; J.-R. Li, J. Sculley and H.-C. Zhou, *Chem. Rev.*, 2012, **112**, 869–932; Y. Cui, Y. Yue, G. Qian and B. Chen, *Chem. Rev.*, 2012, **112**, 1126–1162; L. E. Kreno, K. Leong, O. K. Farha, M. Allendorf, R. P. Van Duyne and J. T. Hupp, *Chem. Rev.*, 2012, **112**, 1105–1125; J. Liu, L. Chen, H. Cui, J. Zhang, L. Zhang and C. Y. Su, *Chem. Soc. Rev.*, 2014, **43**, 6011–6061.

5 D. J. Tranchemontagne, J. L. Mendoza-Cortes, M. O'Keeffe and O. M. Yaghi, *Chem. Soc. Rev.*, 2009, **38**, 1257–1283.

6 Y.-W. Li, J.-R. Li, L.-F. Wang, B.-Y. Zhou, Q. Chen and X.-H. Bu, *J. Mater. Chem. A*, 2013, **1**, 495–499.

7 K. Liu, B. Li, Y. Li, X. Li, F. Yang, G. Zeng, Y. Peng, Z. Zhang, G. Li, Z. Shi, S. Feng and D. Song, *Chem. Commun.*, 2014, **50**, 5031–5033.

8 Y.-X. Tan, Y.-P. He and J. Zhang, *Chem. Commun.*, 2011, **47**, 10647–10649.

9 Y.-X. Tan, Y.-P. He and J. Zhang, *Chem. Mater.*, 2012, **24**, 4711–4716; Z. Fu, J. Lin, L. Wang, C. Li, W. Yan and T. Wu, *Cryst. Growth Des.*, 2016, **16**, 2322–2327; G. Kang, Y. Jeon, K. Y. Lee, J. Kim and T. H. Kim, *Cryst. Growth Des.*, 2015, **15**, 5183–5187.

10 N. C. Burtch and K. S. Walton, *Acc. Chem. Res.*, 2015, **48**, 2850–2857; V. Guillerm, D. Kim, J. F. Eubank, R. Luebke, X. Liu, K. Adil, M. S. Lah and M. Eddaoudi, *Chem. Soc. Rev.*, 2014, **43**, 6141–6172.

11 G. M. Sheldrick, *SHELXTL-NT, version 5.1*, Bruker AXS Inc., Madison, WI, 1997.

12 V. A. Blatov, A. P. Shevchenko and D. M. Proserpio, *Cryst. Growth Des.*, 2014, **14**, 3576–3683.

13 J. Qian, F. Jiang, K. Su, J. Pan, Z. Xue, L. Liang, P. P. Bag and M. Hong, *Chem. Commun.*, 2014, **50**, 15224–15227.

14 Y. Kang, F. Wang, J. Zhang and X. Bu, *J. Am. Chem. Soc.*, 2012, **134**, 17881–17884.

15 X. Luo, Y. Cao, T. Wang, G. Li, J. Li, Y. Yang, Z. Xu, J. Zhang, Q. Huo, Y. Liu and M. Eddaoudi, *J. Am. Chem. Soc.*, 2016, **138**, 786–789; C. W. Zhao, J. P. Ma, Q. K. Liu, X. R. Wang, Y. Liu, J. Yang, J. S. Yang and Y. B. Dong, *Chem. Commun.*, 2016, **52**, 5238–5241.

16 Y. E. Cheon, J. Park and M. P. Suh, *Chem. Commun.*, 2009, 5436–5438; D. J. Xiao, M. I. Gonzalez, L. E. Darago, K. D. Vogiatzis, E. Haldoupis, L. Gagliardi and J. R. Long, *J. Am. Chem. Soc.*, 2016, **138**, 7161–7170; Z. Zhang, S. Xiang, K. Hong, M. C. Das, H. D. Arman, M. Garcia, J. U. Mondal, K. M. Thomas and B. Chen, *Inorg. Chem.*, 2012, **51**, 4947–4953; E. D. Bloch, L. J. Murray, W. L. Queen, S. Chavan, S. N. Maximoff, J. P. Bigi, R. Krishna, V. K. Peterson, F. Grandjean, G. J. Long, B. Smit, S. Bordiga, C. M. Brown and J. R. Long, *J. Am. Chem. Soc.*, 2011, **133**, 14814–14822; M. Dinca and J. R. Long, *J. Am. Chem. Soc.*, 2005, **127**, 9376–93774;

 

P. D. Southon, D. J. Price, P. K. Nielsen, C. J. McKenzie and C. J. Kepert, *J. Am. Chem. Soc.*, 2011, **133**, 10885–10891.

17 S. Ma, X. S. Wang, D. Yuan and H. C. Zhou, *Angew. Chem., Int. Ed.*, 2008, **47**, 4130–4133; Y. E. Cheon and M. P. Suh, *Chem. Commun.*, 2009, **45**, 2296–2298.

18 D. F. Sava Gallis, M. V. Parkes, J. A. Greathouse, X. Zhang and T. M. Nenoff, *Chem. Mater.*, 2015, **27**, 2018–2025.

19 S. Yao, D. Wang, Y. Cao, G. Li, Q. Huo and Y. Liu, *J. Mater. Chem. A*, 2015, **3**, 16627–16632.

20 J. L. C. Rowsell and O. M. Yaghi, *J. Am. Chem. Soc.*, 2006, **128**, 1304–1315; D. F. Sava, V. C. Kravtsov, F. Nouar, L. Wojtas, J. F. Eubank and M. Eddaoudi, *J. Am. Chem. Soc.*, 2008, **130**, 3768–3770; X. Li, X. Chen, F. Jiang, L. Chen, S. Lu, Q. Chen, M. Wu, D. Yuan and M. Hong, *Chem. Commun.*, 2016, **52**, 2277–2280.

21 S. K. Elsaidi, M. H. Mohamed, L. Wojtas, A. Chanthapally, T. Pham, B. Space, J. J. Vittal and M. J. Zaworotko, *J. Am. Chem. Soc.*, 2014, **136**, 5072–5077.

22 Q. M. Wang, D. Shen, M. Bülow, M. L. Lau, S. Deng, F. R. Fitch, N. O. Lemcoff and J. Semanscin, *Microporous Mesoporous Mater.*, 2002, **55**, 217–230.

23 W. Lu, D. Yuan, J. Sculley, D. Zhao, R. Krishna and H. C. Zhou, *J. Am. Chem. Soc.*, 2011, **133**, 18126–18129; S. D. Burd, S. Ma, J. A. Perman, B. J. Sikora, R. Q. Snurr, P. K. Thallapally, J. Tian, L. Wojtas and M. J. Zaworotko, *J. Am. Chem. Soc.*, 2012, **134**, 3663–3666; H. Zhao, Z. Jin, H. Su, J. Zhang, X. Yao, H. Zhao and G. Zhu, *Chem. Commun.*, 2013, **49**, 2780–2782.

24 S. R. Venna and M. A. Carreon, *J. Am. Chem. Soc.*, 2010, **132**, 76–77; H. Wang, X. Zeng and D. Cao, *J. Mater. Chem. A*, 2014, **2**, 11341–11348.

25 Y. He, Z. Zhang, S. Xiang, F. R. Fronczek, R. Krishna and B. Chen, *Chem. Commun.*, 2012, **48**, 6493–6495.

26 Y. Huang, Z. Lin, H. Fu, F. Wang, M. Shen, X. Wang and R. Cao, *ChemSusChem*, 2014, **7**, 2647–2653.

27 R. Krishna, *RSC Adv.*, 2015, **5**, 52269–52295; R. Krishna, *Microporous Mesoporous Mater.*, 2014, **185**, 30–50.

28 J. T. Hughes, D. F. Sava, T. M. Nenoff and A. Navrotsky, *J. Am. Chem. Soc.*, 2013, **135**, 16256–16259.

29 H. Kitagawa, H. Ohtsu and M. Kawano, *Angew. Chem., Int. Ed. Engl.*, 2013, **52**, 12395–12399.

30 M.-H. Zeng, Q.-X. Wang, Y.-X. Tan, S. Hu, H.-X. Zhao, L.-S. Long and M. Kurmoo, *J. Am. Chem. Soc.*, 2010, **132**, 2561–2563.

31 X. Luo, L. Sun, J. Zhao, D.-S. Li, D. Wang, G. Li, Q. Huo and Y. Liu, *Cryst. Growth Des.*, 2015, **15**, 4901–4907.

# Electronic Supplementary Information (ESI)

# Two heterovalent copper–organic frameworks with multiple secondary building units: high performance of gas adsorption and separation, $I_2$ sorption and release

**Shuo Yao,[a] Xiaodong Sun,[a] Bing Liu,[a] Rajamani Krishna,[b] Guanghua Li,[a] Qisheng Huo,[a] and Yunling Liu*[a]**

*a. State Key Laboratory of Inorganic Synthesis and Preparative Chemistry, College of Chemistry, Jilin University, Changchun 130012, P. R. China*

**E-mail: yunling@jlu.edu.cn; Fax: +86-431-85168624; Tel: +86-431-85168614*

*b. Van't Hoff Institute for Molecular Sciences, University of Amsterdam, Science Park 904, 1098 XH Amsterdam, The Netherlands. E-mail: r.krishna@contact.uva.cl.*

**S1. Calculation procedures of selectivity from IAST**

The measured experimental data is excess loadings ($q^{ex}$) of the pure components $CO_2$, $CH_4$, $C_2H_6$ and $C_3H_8$ for **JLU-Liu31**, which should be converted to absolute loadings ($q$) firstly.

$$q = q^{ex} + \frac{pV_{pore}}{ZRT}$$

Here $Z$ is the compressibility factor. The Peng-Robinson equation was used to estimate the value of compressibility factor to obtain the absolute loading, while the measure pore volume 0.85 $cm^3\ g^{-1}$ is also necessary.

The dual-site Langmuir-Freundlich equation is used for fitting the isotherm data at 298K.

$$q = q_{m_1} \times \frac{b_1 \times p^{1/n_1}}{1 + b_1 \times p^{1/n_1}} + q_{m_2} \times \frac{b_2 \times p^{1/n_2}}{1 + b_2 \times p^{1/n_2}}$$

Here $p$ is the pressure of the bulk gas at equilibrium with the adsorbed phase (kPa), $q$ is the adsorbed amount per mass of adsorbent (mol $kg^{-1}$), $q_{m1}$ and $q_{m2}$ are the saturation capacities of sites 1 and 2 (mol $kg^{-1}$), $b_1$ and $b_2$ are the affinity coefficients of sites 1 and 2 (1/kPa), $n_1$ and $n_2$ are the deviations from an ideal homogeneous surface.

The selectivity of preferential adsorption of component 1 over component 2 in a mixture containing 1 and 2, perhaps in the presence of other components too, can be formally defined as

$$S = \frac{q_1/q_2}{p_1/p_2}$$

$q_1$ and $q_2$ are the absolute component loadings of the adsorbed phase in the mixture. These component loadings are also termed the uptake capacities. We calculate the values of $q_1$ and $q_2$ using

the Ideal Adsorbed Solution Theory (IAST) of Myers and Prausnitz.

**S2. Calculations of the isosteric heats of gas adsorption ($Q_{st}$)**

A virial-type expression comprising the temperature-independent parameters $a_i$ and $b_j$ was employed to calculate the enthalpies of adsorption for $CH_4$, $C_2H_6$ and $C_3H_8$ (at 273 and 298 K) on compounds. In each case, the data were fitted using the equation:

$$ln^P = ln^N + {}^1/_T\sum_{i-0}^{m} a_i N^i + \sum_{j-0}^{n} b_j N^j$$

Here, $P$ is the pressure expressed in Torr, $N$ is the amount adsorbed in mmol $g^{-1}$, $T$ is the temperature in K, $a_i$ and $b_j$ are virial coefficients, $m$, $n$ represent the number of coefficients required to adequately describe the isotherms ($m$ and $n$ were gradually increased until the contribution of extra added $a$ and $b$ coefficients was deemed to be statistically insignificant towards the overall fit, and the average value of the squared deviations from the experimental values was minimized). The values of the virial coefficients $a_0$ through $a_m$ were then used to calculate the isosteric heat of adsorption using the following expression.

$$Q_{st} = -R\sum_{i-0}^{m} a_i N^i$$

$Q_{st}$ is the coverage-dependent isosteric heat of adsorption and $R$ is the universal gas constant. The heats of gas sorption for JLU-Liu31 in this manuscript are determined by using the sorption data measured in the pressure range from 0-1 bar (273 and 298 K for gases), which is fitted by the virial-equation very well.

**S3. Supporting Figures**

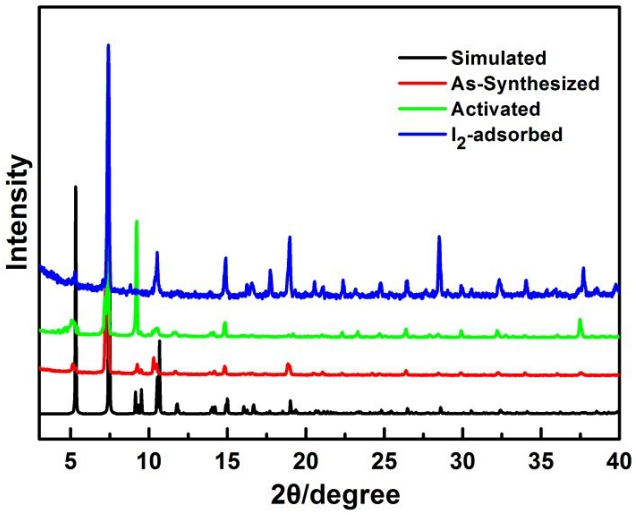


**Fig. S1** PXRD patterns of JLU-Liu31 for simulated, as-synthesized, activated and $I_2$-adsorbed samples. The differences in reflection intensity are probably due to preferred orientations in the powder samples.

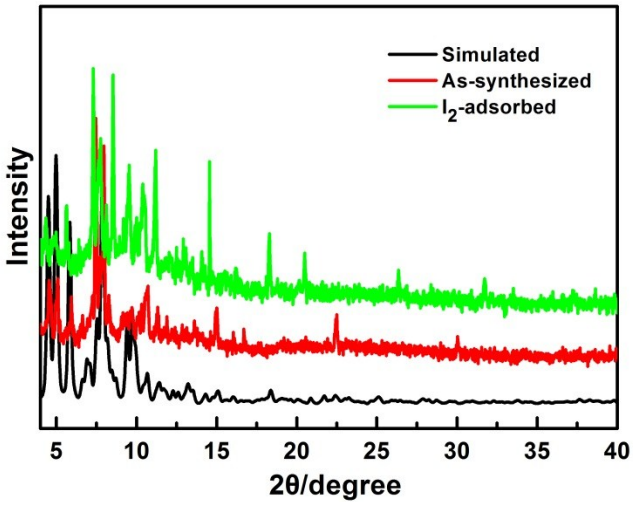


**Fig. S2** PXRD patterns of JLU-Liu32 for simulated, as-synthesized and $I_2$-adsorbed samples. The differences in reflection intensity are probably due to preferred orientations in the powder samples.

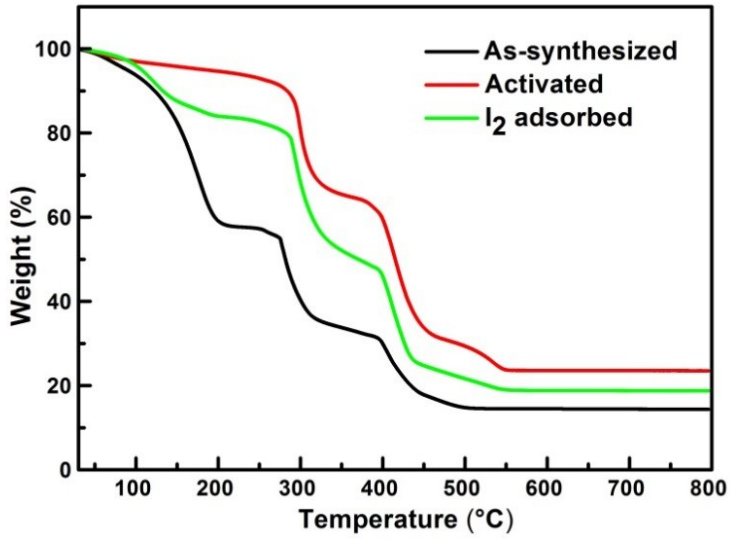


**Fig. S3** TGA curves of JLU-Liu31 for the as-synthesized, activated and iodine adsorbed samples.

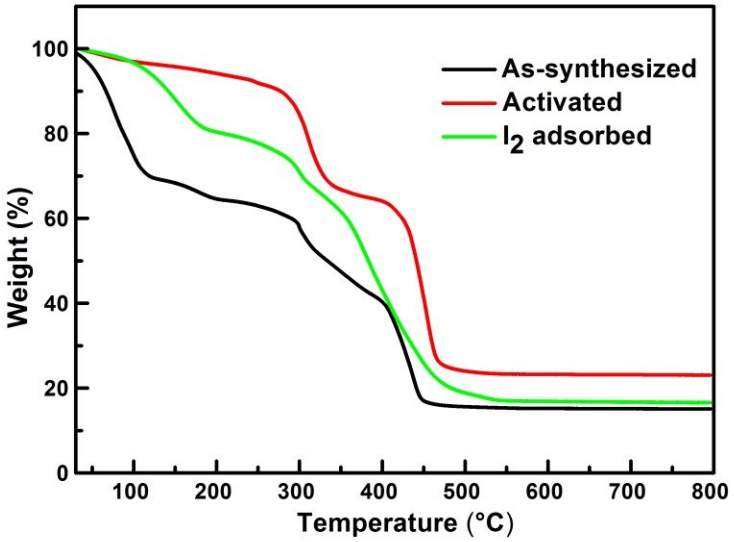


**Fig. S4** TGA curves of JLU-Liu32 for the as-synthesized, activated and iodine adsorbed samples.

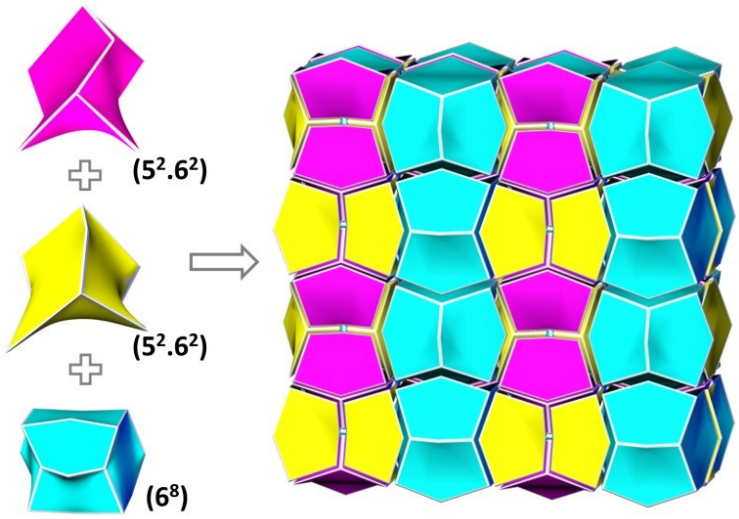


**Fig. S5** Topological features of JLU-Liu31 displayed by tiles and face symbols for pink, yellow and blue tiles are $(5^2.6^2)$, $(5^2.6^2)$ and $(6^8)$.

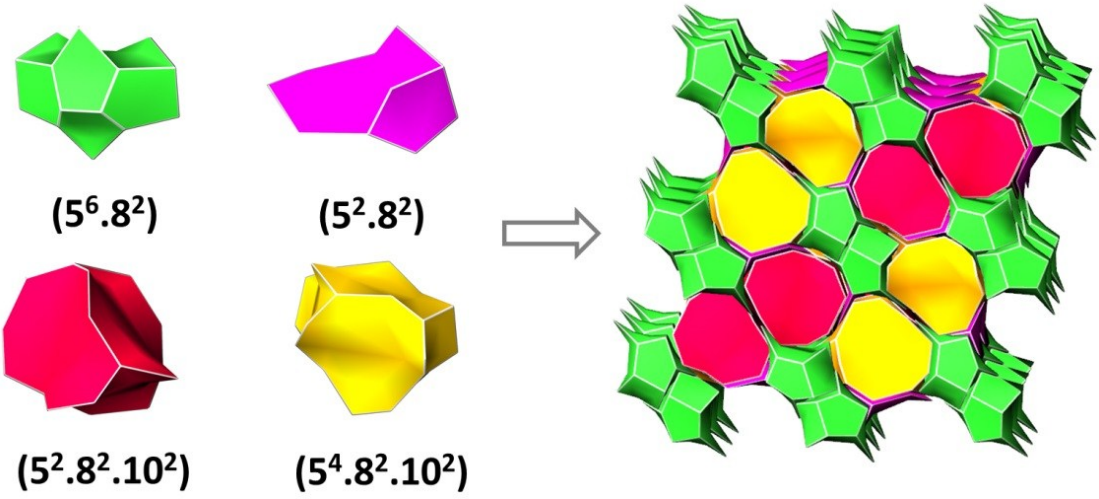


**Fig. S6** Topological features of JLU-Liu32 displayed by tiles and face symbols for green, pink, red and yellow tiles are $(5^6.8^2)$, $(5^2.8^2)$, $(5^2.8^2.10^2)$ and $(5^4.8^2.10^2)$.

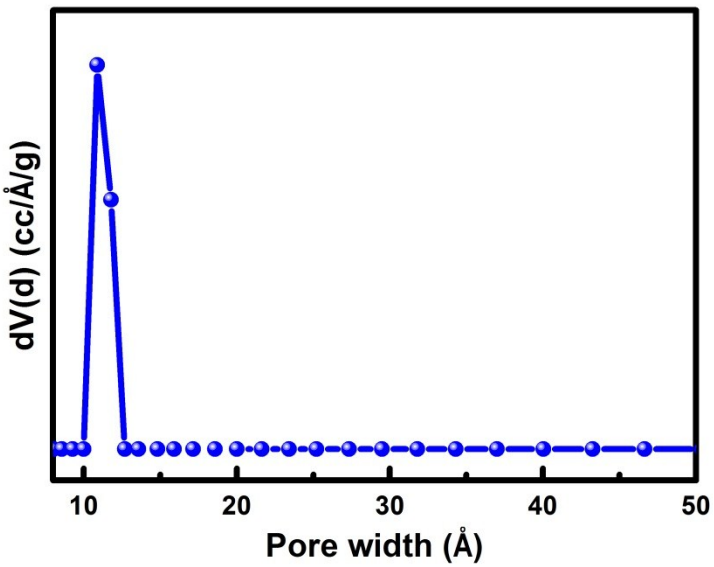


**Fig. S7** The pore size distribution of JLU-Liu31 calculated by using the DFT method.

In order to ensure the accuracy and repeatability of results for the gas adsorption and isosteric heats of JLU-Liu31, we prepare another three batches of samples to make parallel experiments and get another three sets of data for $H_2$, $CO_2$, $CH_4$, $C_2H_6$ and $C_3H_8$. Fig. S8-12 shows the three sets of adsorption isotherms for the five kinds of gases and their isosteric heats calculated by viral method.

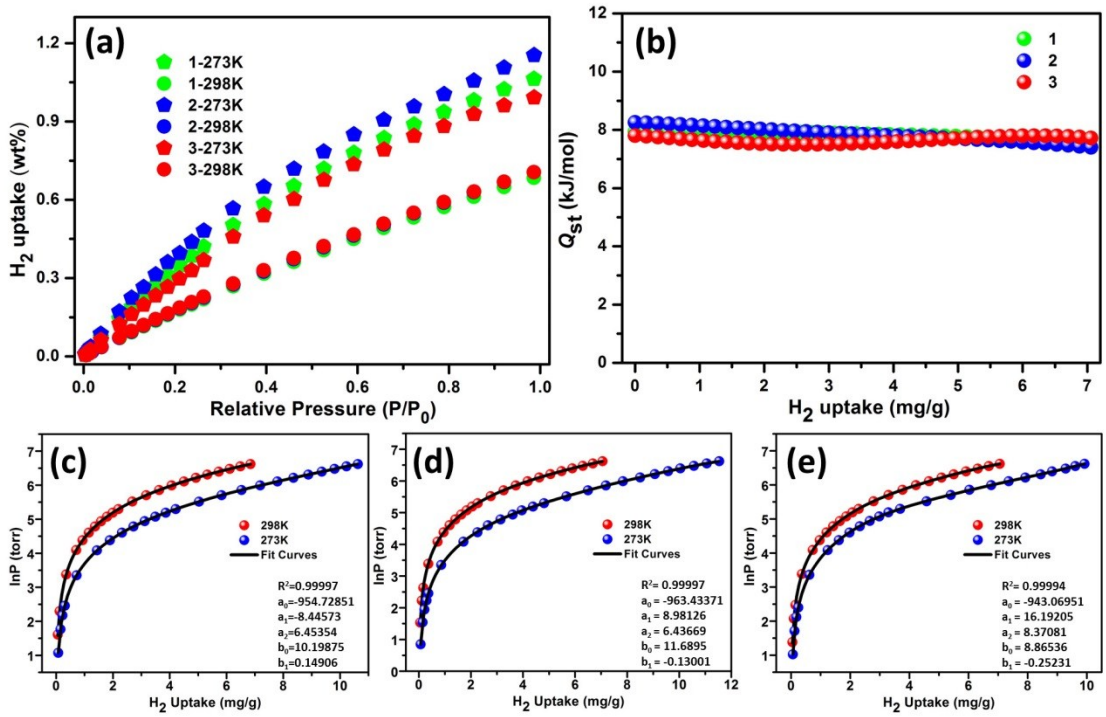


**Fig. S8** (a) $H_2$ sorption isotherms of JLU-Liu31 for three batches of samples at 77 and 87 K; (b) isosteric heats of $H_2$ for the corresponding three samples; (c)-(e) nonlinear curves fitting of $H_2$ for the corresponding three samples.

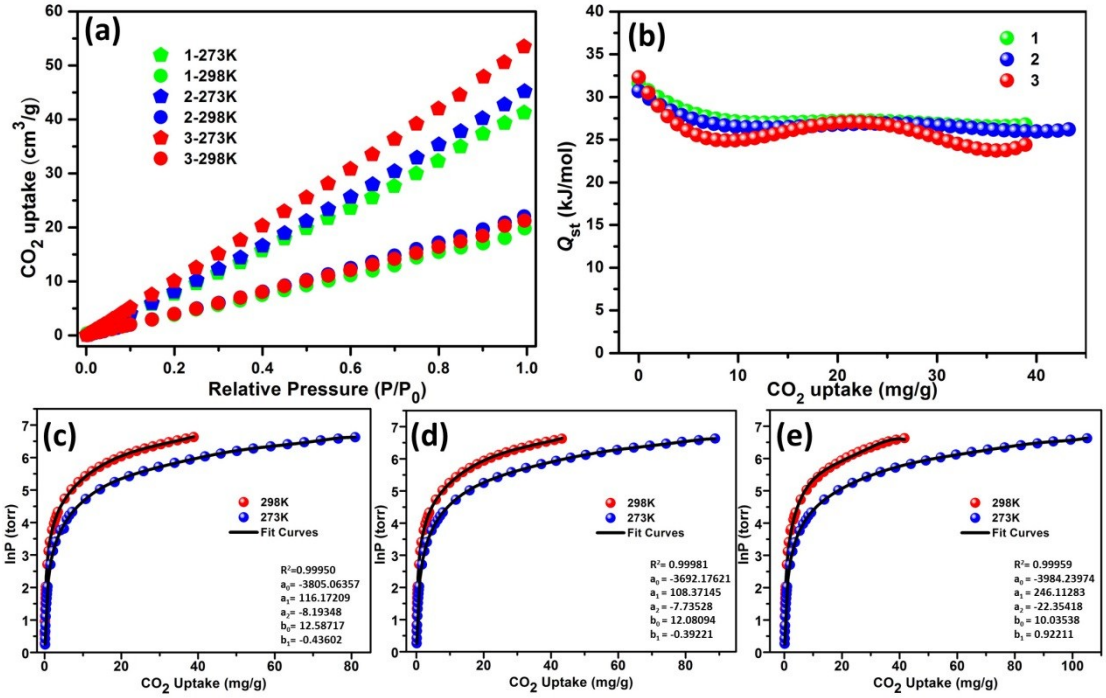


**Fig. S9** (a) $CO_2$ sorption isotherms of JLU-Liu31 for three batches of samples at 273 and 298 K; (b) isosteric heats of $CO_2$ for the corresponding three samples; (c)-(e) nonlinear curves fitting of $CO_2$ for the corresponding three samples.

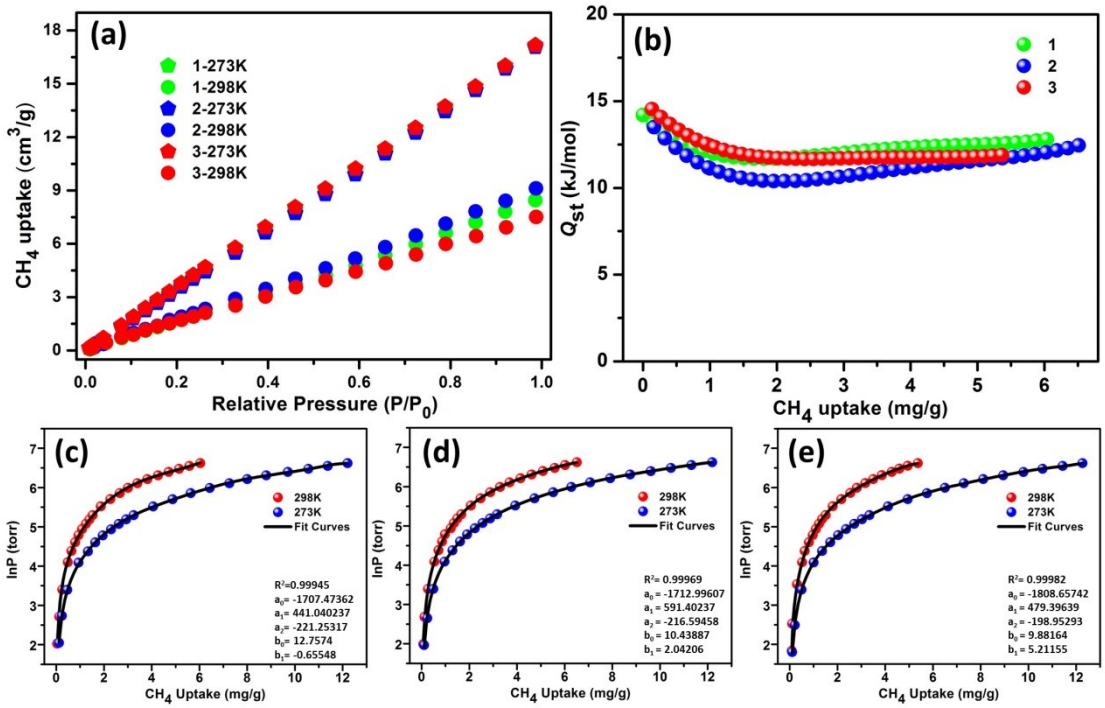


**Fig. S10** (a) $CH_4$ sorption isotherms of JLU-Liu31 for three batches of samples at 273 and 298 K; (b) isosteric heats of $CH_4$ for the corresponding three samples; (c)-(e) nonlinear curves fitting of $CH_4$ for the corresponding three samples.

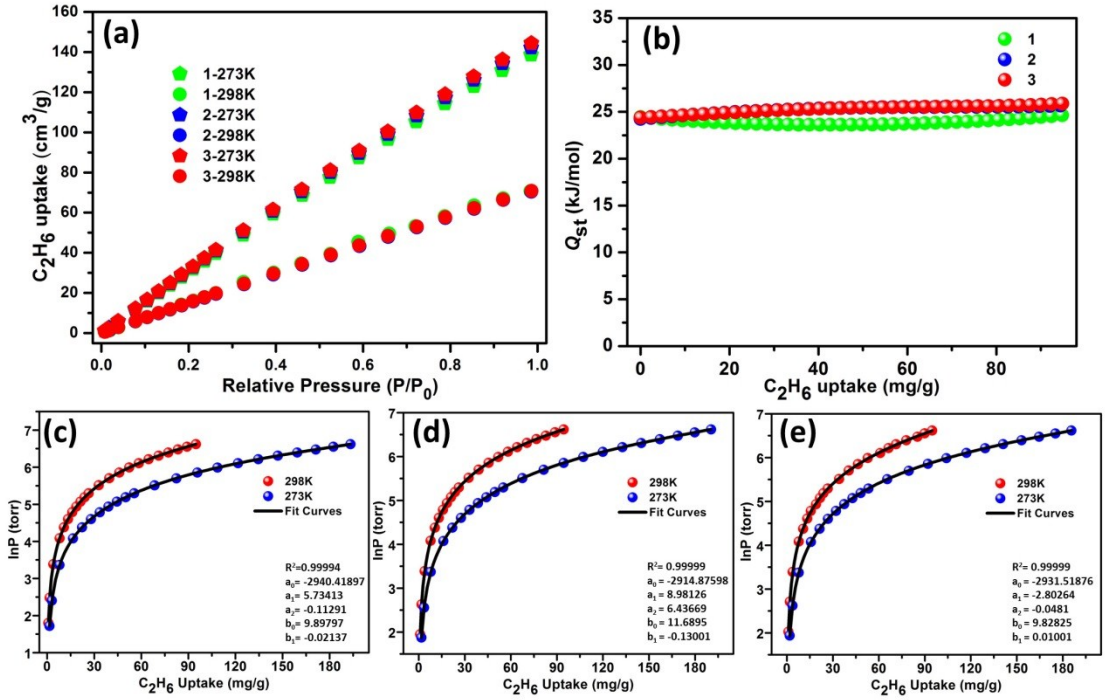


**Fig. S11** (a) $C_2H_6$ sorption isotherms of JLU-Liu31 for three batches of samples at 273 and 298 K; (b) isosteric heats of $C_2H_6$ for the corresponding three samples; (c)-(e) nonlinear curves fitting of $C_2H_6$ for the corresponding three samples.

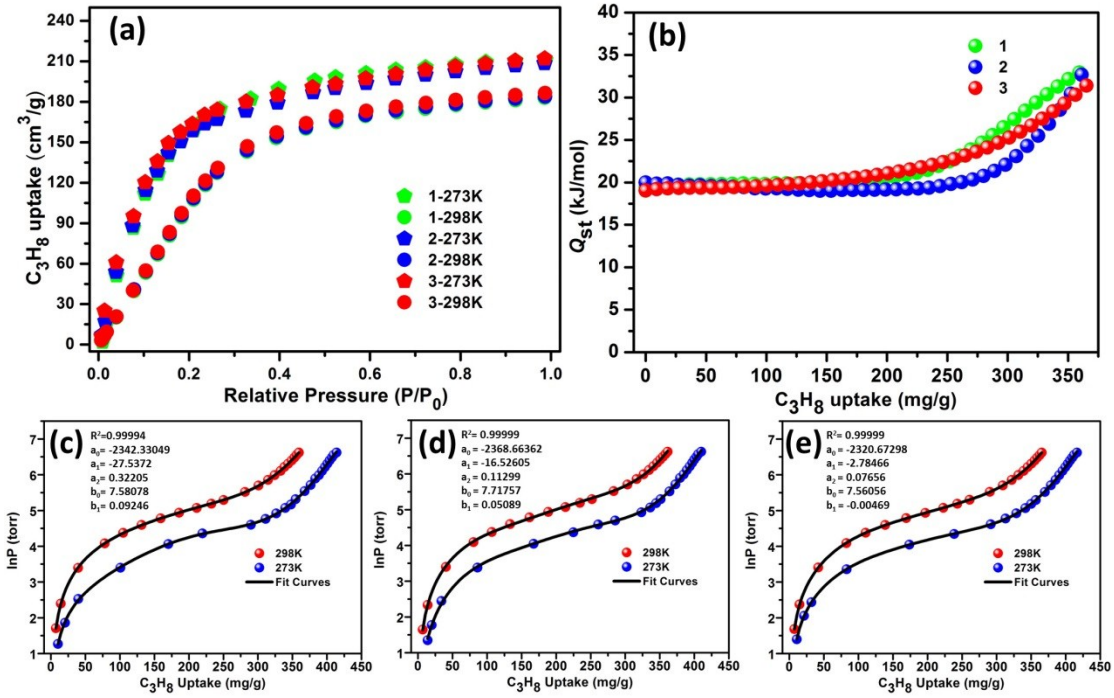


**Fig. S12** (a) $C_3H_8$ sorption isotherms of JLU-Liu31 for three batches of samples at 273 and 298 K; (b) isosteric heats of $C_3H_8$ for the corresponding three samples; (c)-(e) nonlinear curves fitting of $C_3H_8$ for the corresponding three samples.

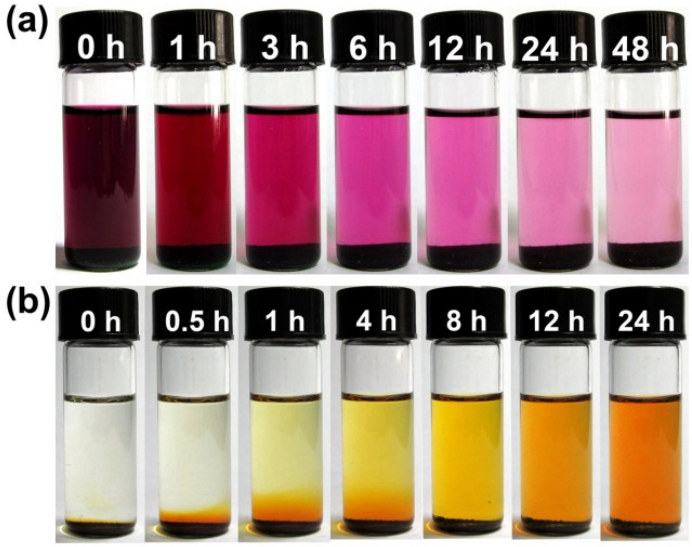


**Fig. S13** (a) Photographs of time-dependent $I_2$ adsorption process of 100 mg JLU-Liu31 in 3mL cyclohexane. (b) Photographs of time-dependent $I_2$ release process of 20 mg JLU-Liu31 in 3 mL ethanol.

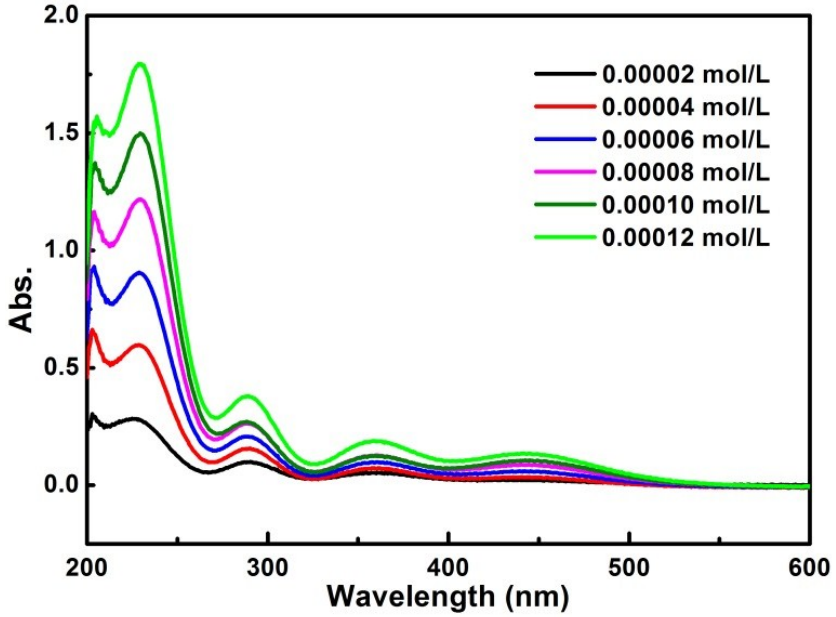


**Fig. S14** UV-vis spectra of iodine in ethanol.

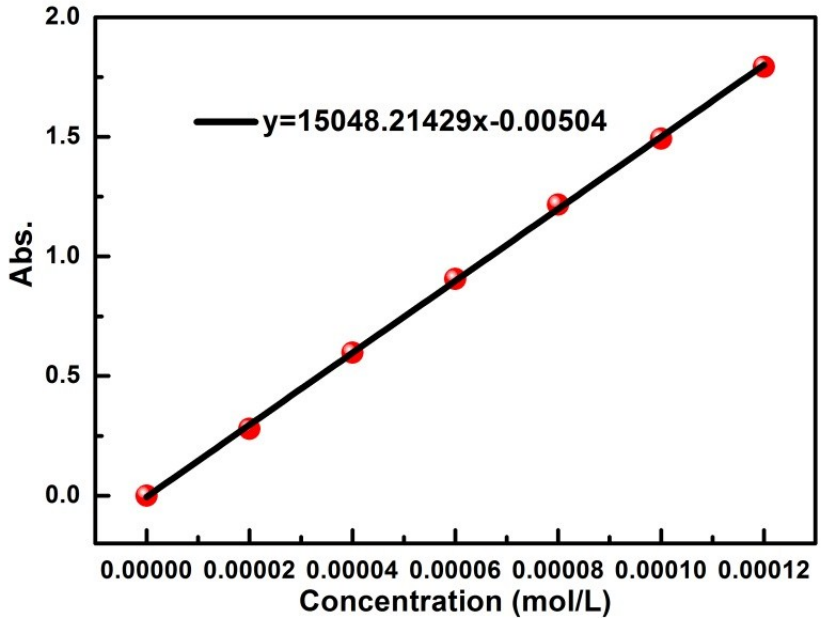


**Fig. S15** Calibration plot of standard iodine by UV-vis spectra.

**S4. Supporting Tables**

**Table S1.** Crystal data and structure refinements for JLU-Liu31 and JLU-Liu32

| compound | **JLU-Liu31** | **JLU-Liu32** |
|---|---|---|
| Formula | $C_{136}H_{180}Cu_8I_4N_{24}O_{32}$ | $C_{123}H_{185}Cu_7I_4N_{27}O_{32}$ |
| Formula weight | 3678.95 | 3506.36 |
| Temperature (K) | 293(2) | 296(2) |
| Wavelength (Å) | 0.71073 | 0.71073 |
| Crystal system | orthorhombic | orthorhombic |
| Space group | *Cmcm* | *Pnnm* |
| *a* (Å) | 33.712(7) | 34.9115(8) |
| *b* (Å) | 19.058(4) | 41.3131(9) |
| *c* (Å) | 33.611(7) | 28.9710(6) |
| $\alpha$ (°) | 90 | 90 |
| $\beta$ (°) | 90 | 90 |
| $\gamma$ (°) | 90 | 90 |
| *V* (Å$^3$) | 21595(7) | 41784.9(16) |
| *Z*, $D_c$ (Mg/m$^3$) | 4,1.132 | 8, 1.116 |
| *F*(000) | 7456 | 14280 |
| $\theta$ range (deg) | 1.208-25.326 | 2.24-19.44 |
| reflns collected/unique | 68324/10118 | 272669/37874 |
| $R_{int}$ | 0.0846 | 0.1228 |
| data/restraints/params | 10118/0/277 | 37874/77/878 |
| GOF on $F^2$ | 1.034 | 0.836 |
| $R_1$, $wR_2$ (I>2σ(I)) | 0.0492, 0.1465 | 0.0499, 0.1173 |
| $R_1$, $wR_2$ (all data) | 0.0750, 0.1575 | 0.1302, 0.1332 |

Since the highly disordered guest molecules were trapped in the channels of the two compounds and could not be modeled properly, there are "Alert level A" about "Check Reported Molecular Weight" and "VERY LARGE Solvent Accessible VOID(S) in Structure" in the "checkCIF/PLATON report" files for JLU-Liu31 and JLU-Liu32. The final formula of JLU-Liu31 and JLU-Liu32 were derived from crystallographic data combined with elemental and thermogravimetric analysis data.

**Table S2.** The topological information for JLU-Liu31 and JLU-Liu32 calculated by TOPOS 4.0 and Systre.

Compound JLU-Liu31

| **Vertex figure** | | | | | | | | | | |
|---|---|---|---|---|---|---|---|---|---|---|
| **Vertex** | CS1 | CS2 | CS3 | CS4 | CS5 | CS6 | CS7 | CS8 | CS9 | CS10 |
| **V1** | 3 | 13 | 29 | 61 | 98 | 148 | 199 | 268 | 334 | 428 |
| **V2** | 3 | 13 | 29 | 59 | 99 | 143 | 201 | 268 | 337 | 421 |
| **V3** | 6 | 18 | 38 | 66 | 108 | 156 | 212 | 272 | 354 | 430 |
| **V4** | 4 | 8 | 28 | 62 | 104 | 140 | 218 | 266 | 352 | 408 |
| **Vertex** | **Extended point symbols** | | | | | | | | | |
| **V1** | [5.5.6(3)] | | | | | | | | | |
| **V2** | [5.5.6(3)] | | | | | | | | | |
| **V3** | [5.5.5.5.6.6.6.6.6.6.6.6.8(4).9(2).9(2)] | | | | | | | | | |
| **V4** | [5.5.5.5.6(2).6(2)] | | | | | | | | | |

Compound JLU-Liu32

| **Vertex figure** | | | | | | | | | | |
|---|---|---|---|---|---|---|---|---|---|---|
| **Vertex** | CS1 | CS2 | CS3 | CS4 | CS5 | CS6 | CS7 | CS8 | CS9 | CS10 |
| **V1** | 3 | 10 | 20 | 42 | 57 | 92 | 135 | 185 | 220 | 282 |
| **V2** | 3 | 10 | 20 | 41 | 63 | 102 | 117 | 179 | 223 | 297 |
| **V3** | 3 | 11 | 21 | 37 | 57 | 99 | 137 | 178 | 224 | 265 |
| **V4** | 5 | 13 | 26 | 36 | 74 | 109 | 151 | 175 | 229 | 297 |
| **V5** | 4 | 8 | 24 | 44 | 70 | 80 | 134 | 154 | 256 | 288 |
| **V6** | 4 | 8 | 24 | 34 | 56 | 84 | 133 | 179 | 219 | 264 |
| **V7** | 6 | 16 | 24 | 40 | 70 | 122 | 154 | 188 | 222 | 292 |
| **V8** | 4 | 9 | 20 | 39 | 70 | 86 | 134 | 183 | 231 | 274 |
| **Vertex** | **Extended point symbols** | | | | | | | | | |
| **V1** | [5.5.8(3)] | | | | | | | | | |
| **V2** | [5.5.8(3)] | | | | | | | | | |
| **V3** | [5.5.5] | | | | | | | | | |
| **V4** | [5.5.5.5.5.8(2).8(2).8(3).8.8] | | | | | | | | | |
| **V5** | [5.5.8.8.11(8).11(8)] | | | | | | | | | |
| **V6** | [5.5.5.8(3).8.8] | | | | | | | | | |
| **V7** | [5.5.5.5.5.5.5.5.8(3).8(3).8(3).8(3).8(2).8(2).8(4)] | | | | | | | | | |
| **V8** | [5.5.5.8(2).5.8(2)] | | | | | | | | | |

**Table S3.** The adsorption amounts of JLU-Liu31 for $H_2$, $CO_2$, $CH_4$, $C_2H_6$ and $C_3H_8$ for four batches of samples.

| | BET ($m^2\ g^{-1}$) | $H_2$ (wt%) | | $CO_2$ ($cm^3\ g^{-1}$) | | $CH_4$ ($cm^3\ g^{-1}$) | | $C_2H_6$ ($cm^3\ g^{-1}$) | | $C_3H_8$ ($cm^3\ g^{-1}$) | |
|---|---|---|---|---|---|---|---|---|---|---|---|
| | | 77K | 87K | 273K | 298K | 273K | 298K | 273K | 298K | 273K | 298K |
| **1** | 1700 | 1.17 | 0.54 | 35 | 17 | 14 | 8 | 142 | 68 | 191 | 169 |
| **2** | 1690 | 1.06 | 0.68 | 41 | 20 | 17 | 8 | 138 | 70 | 210 | 182 |
| **3** | 1610 | 1.15 | 0.70 | 45 | 22 | 17 | 9 | 142 | 70 | 208 | 183 |
| **4** | 1640 | 0.99 | 0.70 | 53 | 21 | 17 | 7 | 144 | 70 | 212 | 186 |

**Table S4.** The $H_2$, $CO_2$, $CH_4$, $C_2H_6$ and $C_3H_8$ isosteric heats of JLU-Liu31 for four batches of samples.

| ` | $H_2$ (kJ/mol) | $CO_2$ (kJ/mol) | $CH_4$ (kJ/mol) | $C_2H_6$ (kJ/mol) | $C_3H_8$ (kJ/mol) |
|---|---|---|---|---|---|
| **1** | 16.8 | 32.6 | 13 | 25 | 20 |
| **2** | 7.9 | 31.6 | 14 | 25 | 19 |
| **3** | 8.0 | 30.7 | 11 | 24 | 20 |
| **4** | 7.8 | 32.3 | 12 | 24 | 19 |

**Table S5.** The refined parameters for the Dual-site Langmuir-Freundlich equations fit for the pure isotherms of $CO_2$, $CH_4$, $C_2H_6$ and $C_3H_8$ for JLU-Liu31 at 298 K.

| | $q_{m1}$ | $b_1$ | $n_1$ | $q_{m2}$ | $b_2$ | $n_2$ | $R^2$ |
|---|---|---|---|---|---|---|---|
| **$CO_2$** | 83.78106 | 0.18044 | 0.00163 | 9.71841E-5 | 1.01298 | 11.14388 | 0.99998 |
| **$CH_4$** | 0.10733 | 2.50388 | 7.60184E-10 | 0.00148 | 4.58951 | 0.97001 | 0.99994 |
| **$C_2H_6$** | 4.43346 | 0.01554 | 0.00688 | 6.52596E-5 | 1.00354 | 1.67025 | 0.99999 |
| **$C_3H_8$** | 2.30909 | 5.99418 | 1.45516E-5 | 0.03516 | 3.79119 | 1.13518 | 0.99999 |